Dalton Transactions

ROYAL SOCIETY OF CHEMISTRY

PAPER

View Article Online
View Journal | View Issue

Check for updates

Cite this: *Dalton Trans.*, 2022, **51**, 2250

Synthesis, molecular structure and fluxional behavior of the elusive $[HRu_4(CO)_{12}]^{3-}$ carbonyl anion†

Cristiana Cesari, *[a] Marco Bortoluzzi, [b] Cristina Femoni, [a] Maria Carmela Iapalucci[a] and Stefano Zacchini [a]

Received 26th October 2021,
Accepted 4th January 2022

DOI: 10.1039/d1dt03622j

rsc.li/dalton

The elusive mono-hydride tri-anion $[HRu_4(CO)_{12}]^{3-}$ (**4**) has been isolated and fully characterized for the first time. Cluster **4** can be obtained by the deprotonation of $[H_3Ru_4(CO)_{12}]^-$ (**2**) with NaOH in DMSO. A more convenient synthesis is represented by the reaction of $[HRu_3(CO)_{11}]^-$ (**6**) with an excess of NaOH in DMSO. The molecular structure of **4** has been determined by single-crystal X-ray diffraction (SC-XRD) as the $[NEt_4]_3$[**4**] salt. It displays a tetrahedral structure of pseudo C_{3v} symmetry with the unique hydride ligand capping a triangular Ru_3 face. Variable temperature (VT) ^1H and $^{13}C\{^1H\}$ NMR experiments indicate that **4** is fluxional in solution and reveal an equilibrium between the C_{3v} isomer found in the solid state and a second isomer with C_s symmetry. Protonation–deprotonation reactions inter-converting $H_4Ru_4(CO)_{12}$ (**1**), $[H_3Ru_4(CO)_{12}]^-$ (**2**), $[H_2Ru_4(CO)_{12}]^{2-}$ (**3**), $[HRu_4(CO)_{12}]^{3-}$ (**4**) and the purported $[Ru_4(CO)_{12}]^{4-}$ (**5**) have been monitored by IR and ^1H NMR spectroscopy. Whilst attempting the optimization of the synthesis of **4**, crystals of $[NEt_4]_2[Ru_3(CO)_9(CO_3)]$ ($[NEt_4]_2$[**7**]) were obtained. Anion **7** contains an unprecedented CO_3^{2-} ion bonded to a zero-valent $Ru_3(CO)_9$ fragment. Finally, the reaction of **6** as the $[N(PPh_3)_2]^+$ ($[PPN]^+$) salt with NaOH in DMSO affords $[Ru_3(CO)_9(NPPh_3)]^-$ (**9**) instead of **4**. Computational DFT studies have been carried out in order to support experimental evidence and the location of the hydride ligands as well as to shed light on possible isomers.

Introduction

Hydridocarbonylates of the Fe–Ru–Os triad played a fundamental role in the development of the chemistry of metal carbonyl clusters.[1–11] The only species structurally characterized for the whole triad are $[HM_3(CO)_{11}]^-$,[12–14] $[HM_4(CO)_{13}]^-$ [15–17] and $[H_2M_4(CO)_{12}]^{2-}$.[10,18,19] In the case of iron, only low nuclearity species comprising 1–5 metal atoms have been structurally characterized, whereas nuclearities up to 10–11 metal atoms have been obtained with Ru and Os (Table 1).[20–22] This is mainly due to the fact that Ru–Ru and Os–Os bonds are stronger than Fe–Fe ones, favoring the formation of larger clusters.[1,2,23] Moreover, the greater sizes of Ru and Os compared to Fe also seem to play a role, allowing the coordination of more ligands to the same metal cage. In this respect, it is noteworthy that $[HRu_4(CO)_{13}]^-$ and $[HOs_4(CO)_{13}]^-$ display a tetrahedral metal cage, whereas $[HFe_4(CO)_{13}]^-$ adopts a more open butterfly structure in order to accommodate all the ligands.[15–17]

It must be remarked that most Ru and Os hydridocarbonylate clusters are neutral or show a low negative charge (charge/nuclearity ≤ 0.5). Conversely, all hydridocarbonylferrates characterized by single crystal X-ray diffraction (SC-XRD) are anionic, often reaching high negative charges (charge/nuclearity = 0.25–1.00). This point is well exemplified by $[H_{4-n}M_4(CO)_{12}]^{n-}$ clusters (M = Fe, Ru, and Os; n = 0–3). Iron clusters of this type have been obtained quite recently and only the di-hydride di-anion $[H_2Fe_4(CO)_{12}]^{2-}$ and mono-hydride tri-anion $[HFe_4(CO)_{12}]^{3-}$ are sufficiently stable in order to be isolated and characterized by SC-XRD.[9,10] In contrast, Ru and Os congeners have been known for a long time, and neutral tetra-hydrides $H_4M_4(CO)_{12}$, tri-hydride mono-anions $[H_3M_4(CO)_{12}]^-$, and di-hydride di-anions $[H_2M_4(CO)_{12}]^{2-}$ (M = Ru, Os) have been structurally characterized.[11,18,19,24,25] Even though there is spectroscopic evidence of their existence, mono-hydride tri-anions $[HM_4(CO)_{12}]^{3-}$ (M = Ru and Os) seem to be rather elusive and they have not been characterized by SC-XRD so far.[26,27]

Besides historical and fundamental aspects, Ru hydride carbonyl clusters are rather interesting from an application point of view.[28] Phosphine derivatives of $H_4Ru_4(CO)_{12}$ as well as other Ru–H–CO clusters are active in homogeneous catalysis.[29–32] For

[a]*Dipartimento di Chimica Industriale "Toso Montanari", Università di Bologna, Viale Risorgimento 4, 40136 Bologna, Italy. E-mail: cristiana.cesari2@unibo.it*
[b]*Dipartimento di Scienze Molecolari e Nanosistemi, Ca' Foscari University of Venice, Via Torino 155, 30175 Mestre (Ve), Italy*

† Electronic supplementary information (ESI) available. CCDC 2115041–2115045. For ESI and crystallographic data in CIF or other electronic format see DOI: 10.1039/d1dt03622j

Table 1 Structurally characterized hydridocarbonylates of Fe, Ru and Os (a complete list of references may be found in the ESI, Table S1†)

Nuclearity	Fe	Ru	Os
1	$[HFe(CO)_4]^-$		
2	$[HFe_2(CO)_8]^-$		
3	$[HFe_3(CO)_{11}]^-$	$[HRu_3(CO)_{11}]^-$	$[HOs_3(CO)_{11}]^-$ $H_2Os_3(CO)_{11}$ $H_2Os_3(CO)_{10}$
4	$[HFe_4(CO)_{13}]^-$	$[HRu_4(CO)_{13}]^-$ $H_2Ru_4(CO)_{13}$	$[HOs_4(CO)_{13}]^-$ $H_2Os_4(CO)_{13}$
	$[HFe_4(CO)_{12}]^{3-}$	$[HRu_4(CO)_{12}]^{3-}$ (this work)	
	$[H_2Fe_4(CO)_{12}]^{2-}$	$[H_2Ru_4(CO)_{12}]^{2-}$ $[H_3Ru_4(CO)_{12}]^-$ $H_4Ru_4(CO)_{12}$	$[H_2Os_4(CO)_{12}]^{2-}$ $[H_3Os_4(CO)_{12}]^-$ $H_4Os_4(CO)_{12}$
5			$H_2Os_5(CO)_{16}$ $[HOs_5(CO)_{15}]^-$
	$[HFe_5(CO)_{14}]^{3-}$		
6			$H_2Os_6(CO)_{19}$
		$[HRu_6(CO)_{18}]^-$ $H_2Ru_6(CO)_{18}$ $H_2Ru_6(CO)_{17}$	$[HOs_6(CO)_{18}]^-$ $H_2Os_6(CO)_{18}$
7			$H_2Os_7(CO)_{22}$ $H_2Os_7(CO)_{21}$
		$[HRu_7(CO)_{20}]^-$	
			$H_2Os_7(CO)_{20}$
8			$[HOs_8(CO)_{22}]^-$
		$[H_2Ru_8(CO)_{21}]^{2-}$	
9			$[HOs_9(CO)_{24}]^-$
10		$[H_2Ru_{10}(CO)_{25}]^{2-}$	
			$[H_4Os_{10}(CO)_{24}]^{2-}$ $[H_5Os_{10}(CO)_{24}]^-$
11		$[HRu_{11}(CO)_{27}]^{3-}$	

instance, $H_4Ru_4(CO)_{12-2x}(P–P)_x$ (x = 1 and 2; P–P = chiral diphosphine) species catalyze several asymmetric isomerization, hydroformylation and hydrogenation reactions.[33–36] Molecular Ru hydride carbonyl clusters may serve also as models in order to help the location of the hydride ligands within Ru nanoparticles employed for hydrogenation.[37,38]

In view of this interest for Ru hydridocarbonylates, we have attempted to isolate and fully characterize the elusive monohydride tri-anion $[HRu_4(CO)_{12}]^{3-}$. Herein, we report its detailed synthesis as well as its first structural characterization by means of SC-XRD. In addition, the fluxional behavior of this cluster in solution has been investigated by variable temperature (VT) ^1H and $^{13}C\{^1H\}$ NMR experiments. Protonation–deprotonation reactions inter-converting $H_4Ru_4(CO)_{12}$ (**1**), $[H_3Ru_4(CO)_{12}]^-$ (**2**), $[H_2Ru_4(CO)_{12}]^{2-}$ (**3**), $[HRu_4(CO)_{12}]^{3-}$ (**4**) and the purported $[Ru_4(CO)_{12}]^{4-}$ (**5**) were monitored by IR and ^1H NMR spectroscopy. Computational DFT studies were carried out in order to support experimental evidence and the location of the hydride ligands as well as to shed light on possible isomers.

Results and discussion

Synthesis, molecular structure and dynamic behavior of $[HRu_4(CO)_{12}]^{3-}$ (4)

It was previously reported that **4** is not stable and it decomposes into a mixture of **3** and **5**, when obtained by deprotonation of **1**.[26] This was likely due to the experimental conditions employed, that is, the reaction of **1** with three equivalents of KH in THF, rather than the intrinsic instability of **4**. Indeed, it was later reported that **4** could be obtained by reaction of **5** with HBr in THF, even if it was not possible to isolate and structurally characterize it.[27]

Seeking a way to isolate and fully characterize such an elusive species, we investigated the reaction of **2** with an excess of NaOH in a highly polar aprotic solvent such as DMSO. This approach was successful, allowing complete crystallographic and spectroscopic characterization of **4**. The same compound could be obtained even more conveniently from the reaction of $[HRu_3(CO)_{11}]^-$ (**6**) with an excess of NaOH in DMSO (Scheme 1). Both these syntheses were inspired by our previous findings on the synthesis of isostructural $[HFe_4(CO)_{12}]^{3-}$ as well as the highly reduced $[Fe_6C(CO)_{15}]^{4-}$.[9,39] Formation of **4** from **2** was just a deprotonation reaction. Conversely, ruthenium was formally reduced from −2/3 to −1 passing from **6** to

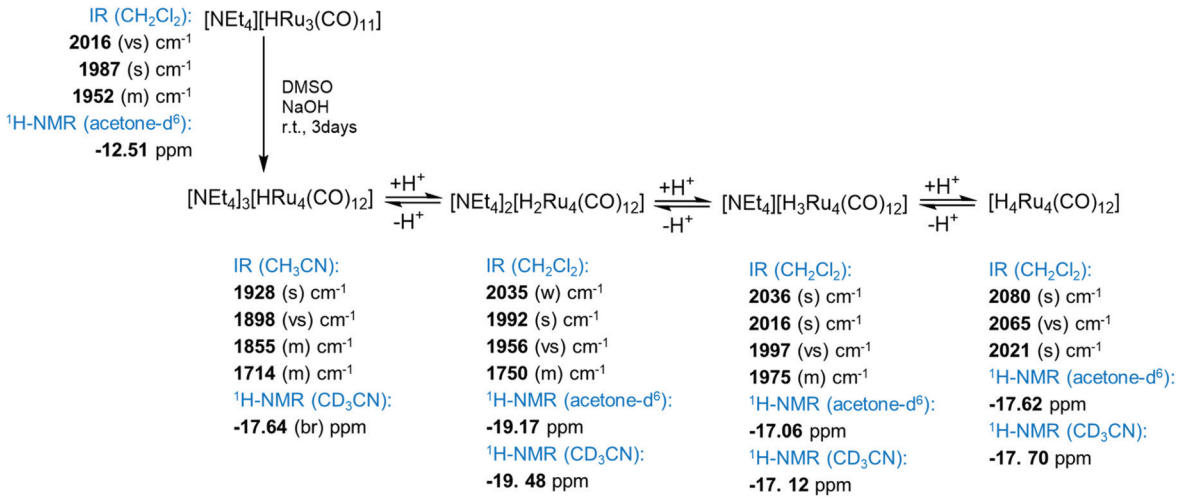

Scheme 1 Synthesis of $[H_{4-n}Ru_4(CO)_{12}]^{n-}$ (n = 0 – 4).

4. Electrons required for reduction were produced by oxidation of CO to CO_2 promoted by OH^- nucleophilic attack at a Ru-coordinated CO ligand. In the presence of an excess of base, CO_2 was converted into CO_3^{2-}. Indeed, we were able to isolate the carbonate-cluster $[Ru_3(CO)_9(CO_3)]^{2-}$ (**7**) as a side product (see the Experimental section for details). After optimization of the synthetic procedure, we were able to isolate **4** as the $[NEt_4]^+$ salt in 77% yields.

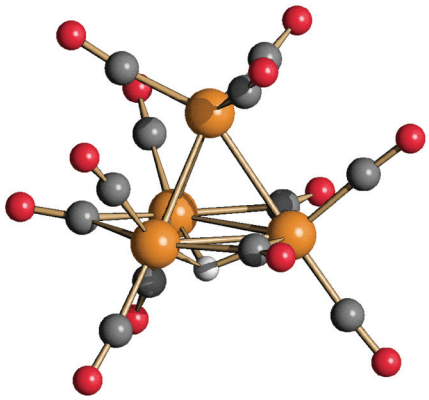

Fig. 1 Molecular structure of $[HRu_4(CO)_{12}]^{3-}$ (**4**) (orange Ru; red O; grey C; and white H).

Table 2 Main bond distances of $[HRu_4(CO)_{12}]^{3-}$ (**4**) compared to $[H_3Ru_4(CO)_{12}]^-$ (**2**) (C_2 and C_{3v} isomers) and $[H_2Ru_4(CO)_{12}]^{2-}$ (**3**). See Scheme 2 for labelling

	4	**3**[a]	**2** (C_2 isomer)[b]	**2** (C_{3v} isomer)[b]
Ru(1)–Ru(2)	2.8032(11)	2.9771(4)	2.9032(5)	2.7733(5)
Ru(1)–Ru(3)	2.8001(11)	2.9558(4)	2.7871(5)	2.7753(5)
Ru(1)–Ru(4)	2.8018(11)	2.8183(4)	2.7614(5)	2.7841(4)
Ru(2)–Ru(3)	2.8106(11)	2.7735(4)	2.9423(4)	2.9380(5)
Ru(2)–Ru(4)	2.8006(11)	2.7842(4)	2.7919(4)	2.9218(5)
Ru(3)–Ru(4)	2.8113(11)	2.7526(4)	2.9167(5)	2.9191(4)
H(1)–Ru(1)	—	1.71(4)	1.73(4)	—
H(1)–Ru(2)	1.78(4)	1.86(4)	1.77(4)	1.75(4)
H(1)–Ru(3)	1.77(4)			
H(1)–Ru(4)	1.78(4)	—	—	1.83(4)
H(2)–Ru(2)	—	—	1.79(4)	1.74(4)
H(2)–Ru(3)	—	1.87(4)	1.72(4)	1.76(4)
H(2)–Ru(1)	—	1.64(4)	—	—
H(3)–Ru(3)	—	—	1.72(4)	1.72(4)
H(3)–Ru(4)	—	—	1.80(4)	1.76(4)

[a] From ref. 11 and 18. [b] From ref. 11 and 24.

The molecular structure of **4** was determined by SC-XRD (Fig. 1 and Table 2). Moreover, **4** was spectroscopically characterized by IR and VT ^1H NMR techniques. In order to gain further insights into its behavior in solution, VT $^{13}C\{^1H\}$ NMR experiments were performed on a ^{13}CO-enriched sample (*ca.* 50%) prepared from $[HRu_3(^{13}CO)_{11}]^-$ (**6–^{13}CO**).

The structure of **4** closely resembles that of $[HFe_4(CO)_{12}]^{3-9}$ and displays an idealized C_{3v} symmetry. It consists of a tetrahedral Ru_4 cage and the unique hydride is μ_3-coordinated to the triangular basal face. The apical Ru atom is bonded to three terminal carbonyls, whereas each of the three Ru atoms on the basal plane is bonded to two terminal CO ligands. The three remaining carbonyl ligands are in edge bridging positions on the basal triangle. The stereochemistry of the CO ligands of **4** is similar to that of **3**,[11,18] which contains two edge bridging μ-H hydride ligands on two different Ru_{apical}–Ru_{basal} edges. In contrast, **2** exists in solution as well as in the solid state as two isomers (C_2 and C_{3v}) and both contain only terminal carbonyls and edge bridging hydrides.[11,24] In agreement with the solid state structure, the IR spectrum of the CH_3CN solution of **4** (Fig. S1 in the ESI†) displays three ν_{CO} bands in the terminal region [1928(s), 1898(vs) and 1855(m) cm^{-1}] and one in the edge-bridging region [1714(m) cm^{-1}].

The six Ru–Ru bonding contacts of **4** are comprised in a rather narrow range [2.8001(11)–2.8113(11) Å] even if they have different environments. Indeed, three of them [Ru(1)–Ru(2), Ru(1)–Ru(3) and Ru(1)–Ru(4), see Scheme 2 for labeling] are not bridged by any ligand, whereas the three Ru–Ru edges on the basal triangle [Ru(2)–Ru(3), Ru(3)–Ru(4), Ru(2)–Ru(4)] are bridged by three μ-CO ligands and the resulting triangular face is capped by a μ_3-H. The shortening of the Ru–Ru distances expected because of the μ-CO ligands is compensated by the elongation due to the face capping hydride, making these three Ru–Ru contacts similar to the non-bridged ones. Indeed, in the case of **3**, where the two μ-H and three μ-CO ligands are located on different edges, it is possible to distinguish three sets of Ru–Ru distances.[11,18] The two edges bridged by hydride ligands [2.9558(4) and 2.9771(4) Å] are considerably elongated as expected, whereas the three Ru–Ru edges supported by μ-CO ligands [2.7526(4)–2.7842(4) Å] are shortened. The unique Ru–Ru edge not bearing any bridging ligand displays an intermediate value [2.8183(4) Å], very similar to those found in **4**. In

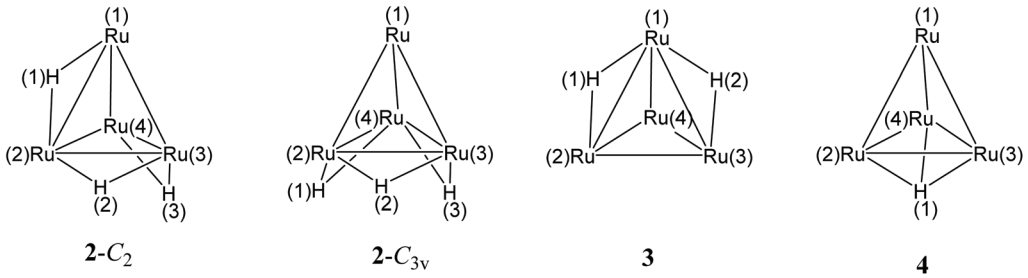

Scheme 2 Labelling of $[H_3Ru_4(CO)_{12}]^-$ (**2**) (C_2 and C_{3v} isomers), $[H_2Ru_4(CO)_{12}]^{2-}$ (**3**), and $[HRu_4(CO)_{12}]^{3-}$ (**4**) (CO omitted for clarity).

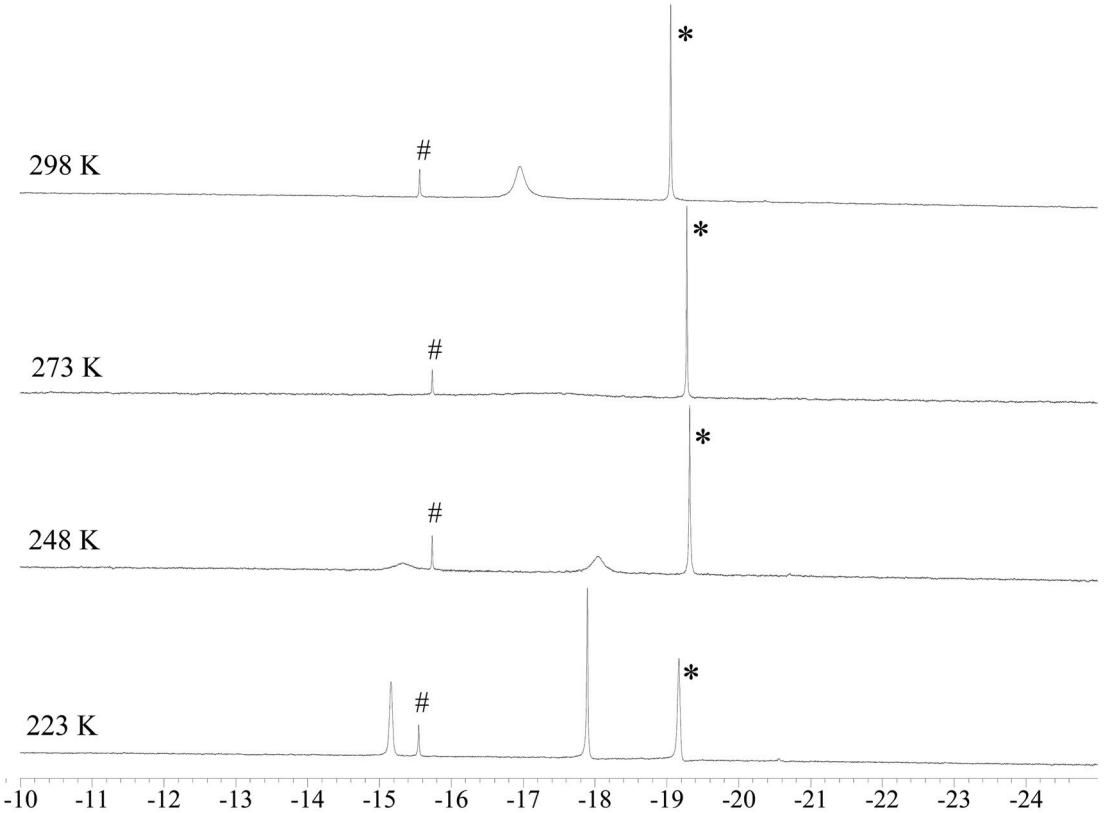

Fig. 2 Hydride region of the VT ^{1}H NMR spectra of $[NEt_4]_3[HRu_4(CO)_{12}]$ (**4**) in DMF-d^7. * $[H_2Ru_4(CO)_{12}]^{2-}$ (**3**). #, unknown impurity.

the case of **2** (C_2 and C_{3v} isomers), since all carbonyls are terminally coordinated, there are only two sets of Ru–Ru contacts: those bridged by μ-H ligands [2.9032(5)–2.9423(4) Å, C_2 isomer; 2.9191(4)–2.9380(5) Å, C_{3v} isomer] are longer than the unbridged ones [2.7614(5)–2.7919(4) Å, C_2 isomer; 2.7735(5)–2.7841(4) Å, C_{3v} isomer].[11,24]

The ^{1}H NMR spectrum of **4** recorded at 298 K (Fig. 2 and Fig. S8 in the ESI†) displays broad resonances at −17.65 and −17.95 ppm in CD_3CN and DMF-d^7 solutions, respectively. The sharp singlets at −15.56 and −19.06 ppm (in DMF-d^7 solution) are due to an unknown impurity and **3**, respectively. The presence of **3** is due to the fact that **4** is easily protonated (see below for details). Upon lowering the temperature, complete coalescence of the resonance of **4** is observed at 273 K and, then, two resonances appear at lower temperatures. The slow exchange limit is reached at 223 K in DMF-d^7 solution, where two singlets at −17.90 and −15.16 ppm are present in a 1.2 : 1 ratio. The presence of two resonances in the hydride region can be explained by assuming that two exchanging isomers of **4** are present in solution.

Kinetic constants for the exchange process in DMF-d^7 solution at different temperatures (Table 3) were obtained by line-shape analysis using the gNMR 5.0.6.0 program for the simulation of VT ^{1}H NMR spectra.[40] The Eyring plot yields the following values for the activation parameters: $\Delta H^{\ddagger}$ = +43 ± 6 kJ mol^{-1} and $\Delta S^{\ddagger}$ = −14 ± 24 J K^{-1} mol^{-1}. The precision of the entropy term does not allow us to determine if it is zero, positive or negative. In all cases, we could expect a value close to zero. These activation parameters are comparable to those reported for the rapid inter-conversion of the C_2 and C_{3v} isomers of **2**, that is, $\Delta H^{\ddagger}$ = +46 kJ mol^{-1} and $\Delta S^{\ddagger}$ = 0.2–8 J K^{-1} mol^{-1}.[41]

Table 3 Kinetic constants at different temperatures for the exchange between the two isomers of $[HRu_4(CO)_{12}]^{3-}$ (**4**) in DMF-d^7 solution as obtained from the line-shape analysis of VT ^{1}H NMR spectra

T	k
298 K	6.0×10^4 s^{-1}
273 K	3.5×10^3 s^{-1}
248 K	8.0×10^3 s^{-1}
223 K	1.0×10^2 s^{-1}

In order to gain further insight into the structures of the two isomers of **4**, VT $^{13}C\{^1H\}$ NMR experiments were performed on a ^{13}CO-enriched (*ca.* 50%) sample prepared using **6–^{13}CO** (Fig. 3). The $^{13}C\{^1H\}$ NMR spectrum recorded at 298 K displays, in the carbonyl region, a broad resonance at *ca.* 226 ppm in agreement with the fluxional behavior observed in the VT ^{1}H NMR experiments. Some sharp resonances are also observed, due to the abovementioned impurities. Moreover, the broad resonance at *ca.* 220 ppm is attributable to **3**. Upon lowering the temperature to 223 K, the broad resonance of **4** is split into several resonances. Four sharp resonances are clearly visible at 268.7, 213.4, 213.0, and 201.7 ppm in a 1 : 1 : 1 : 1 ratio, with the first resonance corresponding to the μ-CO

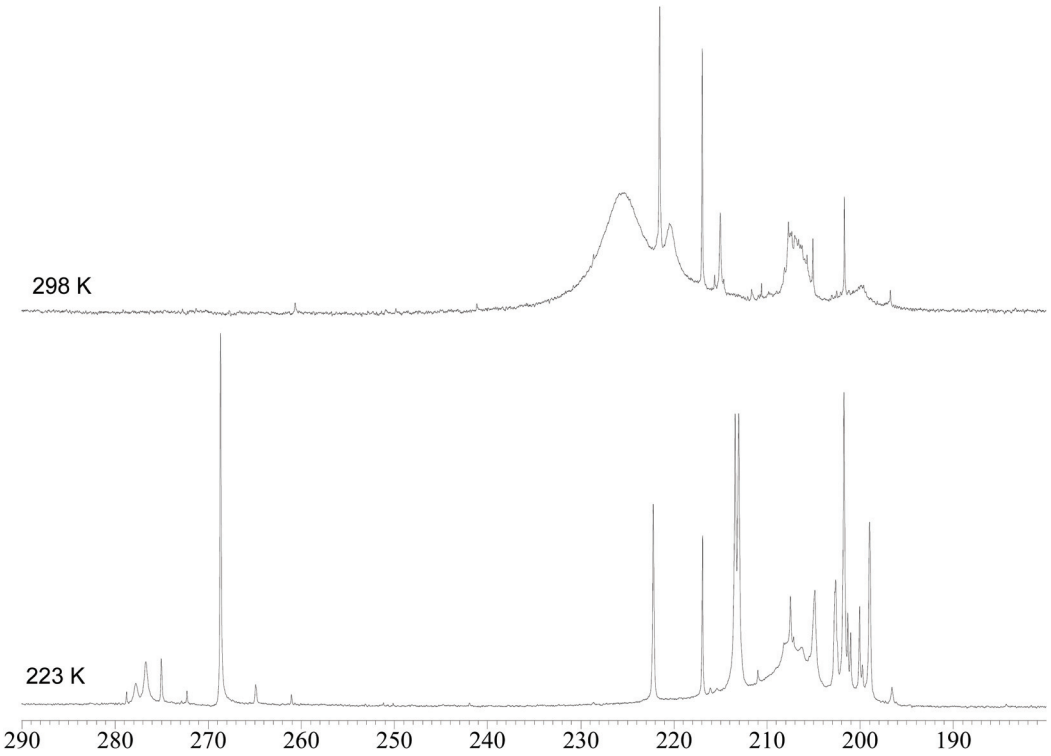

Fig. 3 Carbonyl region of the $^{13}C\{^1H\}$ NMR spectra of $[NEt_4]_3[HRu_4(CO)_{12}]$ (**4**) in DMF-d^7 at 298 K and 223 K. The sample has been enriched with ^{13}CO.

ligands and the other three resonances to terminal carbonyls. These NMR features are in agreement with the C_{3v} symmetry of the major isomer found also in the solid state structure of **4**. A similar low temperature $^{13}C\{^1H\}$ NMR spectrum was previously reported for $[HFe_4(CO)_{12}]^{3-}$.[9]

Regarding the second isomer, it must be remarked that, in the $^{13}C\{^1H\}$ NMR spectrum recorded at 223 K, two further resonances in the μ-CO region are present at 277.8 and 276.7 in a 1 : 2 ratio. Thus, it can be supposed that the second isomer retains the same stereochemistry of the CO ligands (9 terminal and 3 edge-bridging), whereas the unique hydride is now bridging one Ru_{apical}–Ru_{basal} edge, lowering the symmetry from C_{3v} to C_s. Because of the C_s symmetry, the three μ-CO ligands are not equivalent but split into two sets composed of one and two carbonyls, respectively, as spectroscopically observed. The same should apply also to the terminal CO ligands resulting in six resonances with relative intensities in a ratio of 1 : 2 : 1 : 2 : 1 : 2. Indeed, several resonances are present at low temperatures in the 195–220 ppm region but, because of the presence of **3** as well as other impurities, it is not possible to fully assign them.

The location of the hydride in the C_{3v} isomer of **4** was confirmed using DFT calculations (Fig. 4). Moreover, the computational simulations allowed us to optimize the second isomer of **4** with a rough C_s symmetry (R = 0.019), in agreement with the NMR data. The coordination mode of the hydride in the C_s isomer is μ-H, bridging the apical Ru and one of the basal Ru centers. The energies of the two isomers are comparable in the limits of the computational model applied, according to the NMR integration of the hydride resonances (Fig. 2). It is worth noting that in the absence of intermolecular interactions, the C_s isomer is predicted to be slightly more stable than the C_{3v} one.

The stepwise protonation of **4** with $HBF_4{\cdot}Et_2O$ affords the previously reported **3**, **2**, and **1**. The reaction has been monitored by IR and ^1H NMR spectroscopy (Fig. 5 and 6; Fig. S1–S5 and S9 in the ESI†). As mentioned above, **4** is a strong base and is readily protonated. Indeed, its ^1H NMR spectrum is always contaminated by significant amounts of **3**. After the addition of one mole equivalent of acid, **4** completely reacts and the ^1H NMR spectrum displays the presence of **3** accompanied by a small amount of **2**. The addition of a second mole equivalent of $HBF_4{\cdot}Et_2O$ quantitatively converts **3** into **2** with a small amount of **1**. The latter becomes the unique species in solution after the addition of a third mole equivalent of acid. Because of the strong basicity of **4**, all attempts to deprotonate it and isolate the tetra-anion **5** failed.

In order to shed light on the different stability of $[H_{4-n}Ru_4(CO)_{12}]^{n-}$ compared to $[H_{4-n}Fe_4(CO)_{12}]^{n-}$, the energy variation associated with the reaction $[H_{4-n}Ru_4(CO)_{12}]^{n-}$ + $[H_{4-m}Fe_4(CO)_{12}]^{m-}$ → $[H_{4-m}Ru_4(CO)_{12}]^{m-}$ + $[H_{4-n}Fe_4(CO)_{12}]^{n-}$ (n = 1, 2, 3; $m = n - 1$) was studied. Negative energy variations indicate the higher basicity of the ruthenium cluster with respect to the related iron species. For the sake of comparison, the same isomer was considered for changing the metal centre (see Fig. 7). As reported in Fig. 7, ruthenium clusters were in

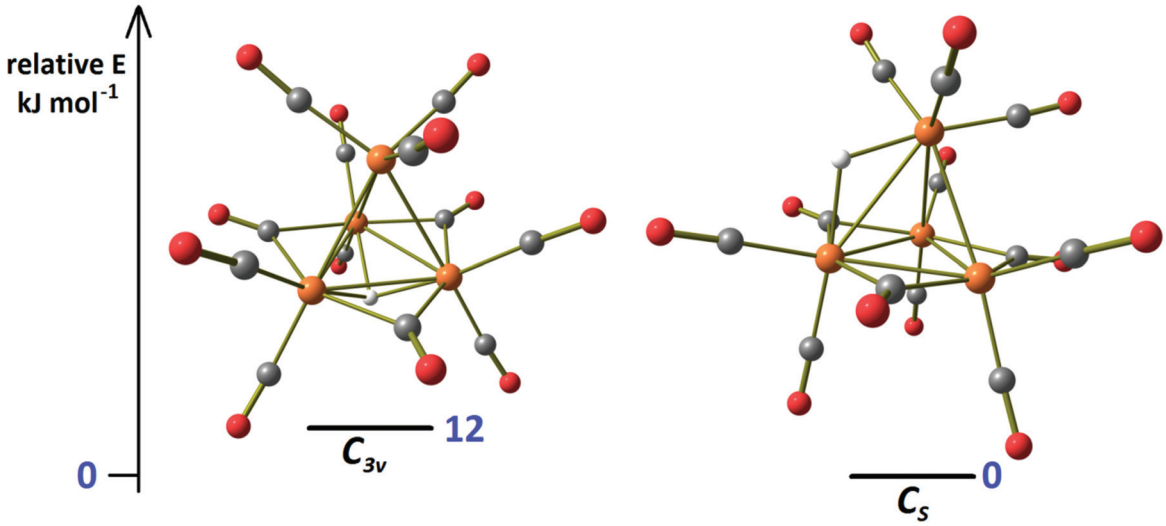

Fig. 4 DFT-optimized isomers of cluster **4** and relative energy values (orange Ru; red O; grey C; and white H).

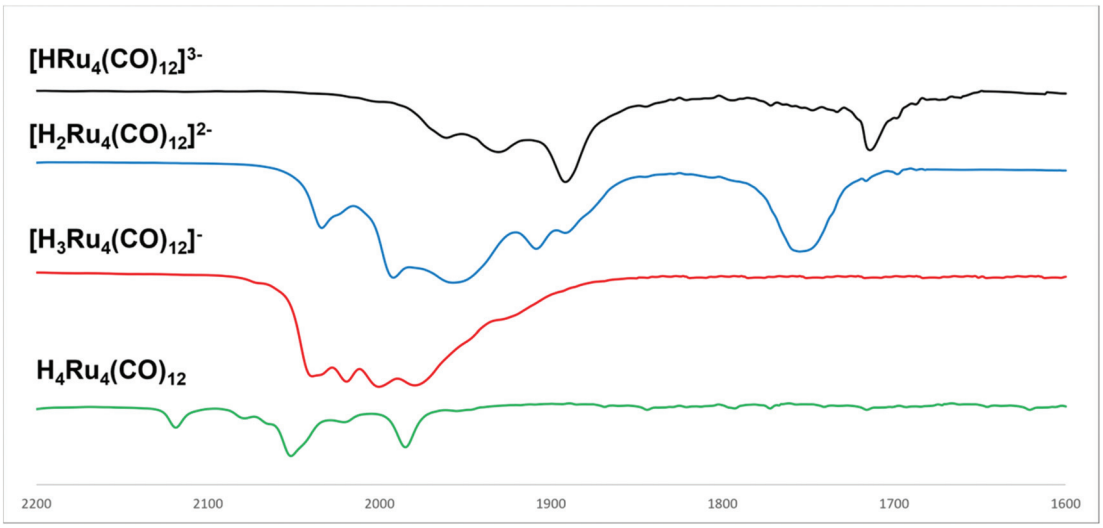

Fig. 5 IR spectra in the ν_{CO} region of $[H_{4-n}Ru_4(CO)_{12}]^{n-}$ (n = 0–3) obtained from the stepwise protonation of $[HRu_4(CO)_{12}]^{3-}$ (**4**) with $HBF_4{\cdot}Et_2O$ in CH_3CN.

all cases more basic than the related iron species, and the relative basicity increased with the number of coordinated hydrides.

As mentioned at the beginning of this section, **7** was obtained as a side product during the synthesis of **4** starting from **6**. Its formation is likely due to the partial decomposition of **6** which formally results in a zero-valent unsaturated "$Ru_3(CO)_9$" fragment. The latter can bind a CO_3^{2-} ion which, in turn, is formed from the oxidation of CO to CO_2 and subsequent reaction with OH^-. This may be viewed as an indirect proof of the fact that **6** is reduced to **4** by oxidation of CO in the presence of OH^- ions.

The molecular structure of **7** (Fig. 8) is rather unique as it contains the first example of a CO_3^{2-} ion bonded to (formally) zero-valent metal atoms. Indeed, the carbonate ion is usually found bonded, also as a multidentate ligand, to metals in a formal positive oxidation state.[11,42] In particular, the CO_3^{2-} ion of **7** is bonded to one Ru atom *via* one O-atom and to two further Ru atoms through a second (edge bridging) O-atom, whereas the third oxygen is not bonded to any metal atom. Three CO ligands are edge bridging on the Ru_3 triangle and, in addition, there are two terminal carbonyls on each Ru atom.

The coordination mode of the carbonate ion was confirmed using DFT calculations. The root-mean-square deviation (RMSD) between X-ray and DFT-optimized structures is only 0.019 Å. Three Ru–O (3,–1) bond critical points (b.c.p.) were obtained from the atom-in-molecule (AIM) analysis of the cluster (Fig. 8). The computed Mayer bond order for the Ru–(κ^1-O) bond is 0.575, while the bond order for the two Ru–(μ-O) bonds is lower (0.437). In agreement with this result, the elec-

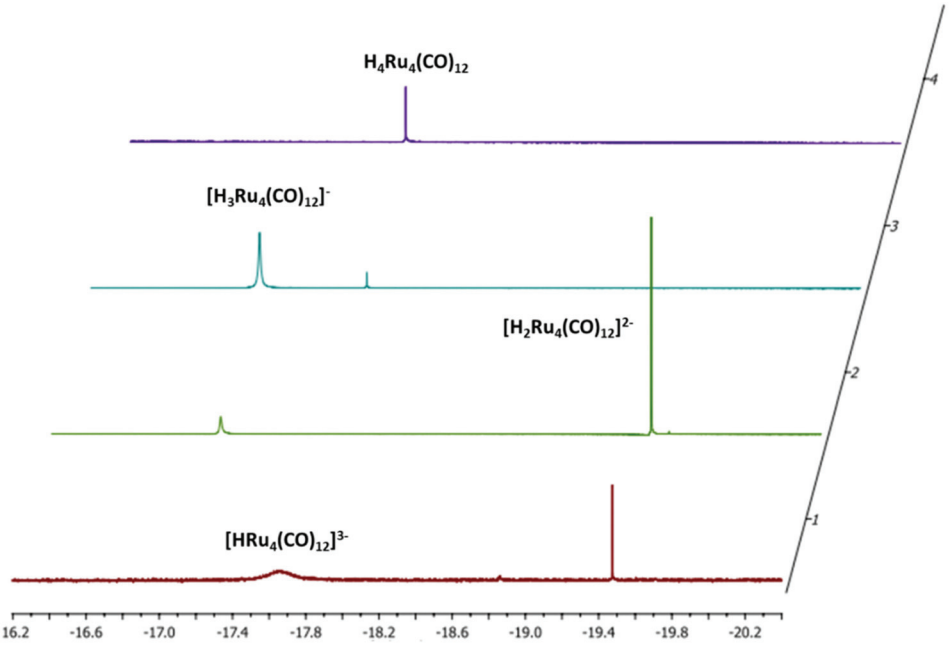

Fig. 6 Hydride region of the ^{1}H NMR spectra of $[H_{4-n}Ru_4(CO)_{12}]^{n-}$ (n = 0–3) obtained from the stepwise protonation of $[HRu_4(CO)_{12}]^{3-}$ (**4**) with $HBF_4{\cdot}Et_2O$ in CD_3CN at 298 K.

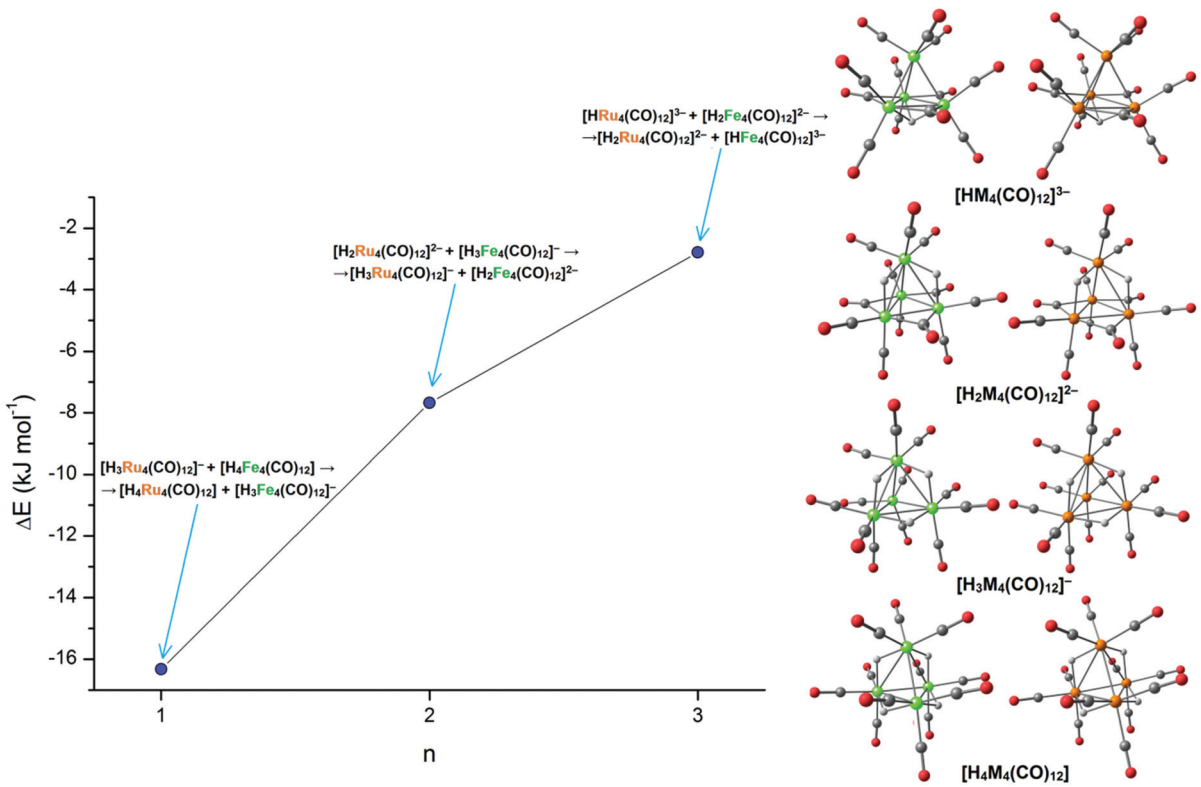

Fig. 7 Energy variations for the reactions $[H_{4-n}Ru_4(CO)_{12}]^{n-} + [H_{4-m}Fe_4(CO)_{12}]^{m-} \rightarrow [H_{4-m}Ru_4(CO)_{12}]^{m-} + [H_{4-n}Fe_4(CO)_{12}]^{n-}$ ($m = n - 1$) and DFT-optimized structures of the isomers considered (green Fe; orange Ru; red O; grey C; and white H).

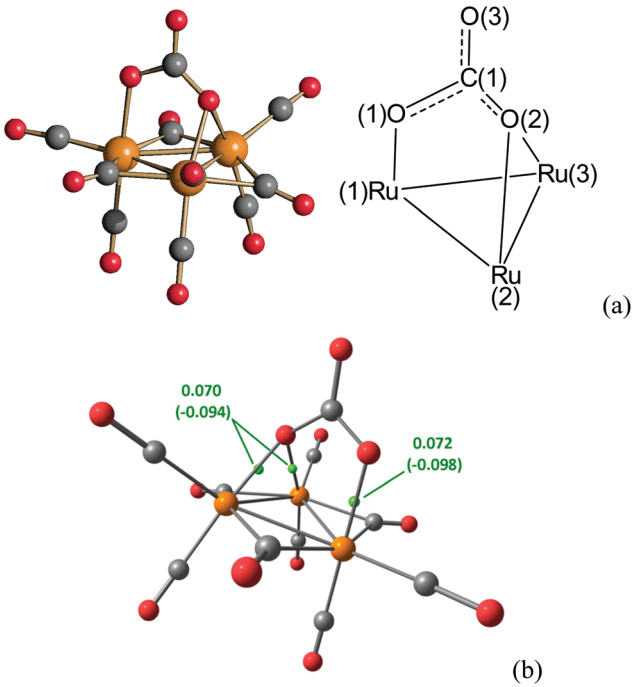

Fig. 8 (a) Molecular structure of $[Ru_3(CO)_9(CO_3)]^{2-}$ (**7**) (orange Ru; red O; grey C) with a labeling scheme. Main bond distances (Å) and angles (°): Ru(1)–Ru(2) 2.790(3), Ru(1)–Ru(3) 2.800(2), Ru(2)–Ru(3) 2.634(2), Ru(1)–O(1) 2.147(14), Ru(2)–O(2) 2.149(13), Ru(3)–O(12) 2.174(13), C(1)–O(1) 1.34(3), C(1)–O(2) 1.28(3), C(1)–O(3) 1.22(3), Ru(1)–O(1)–C(1) 117.9(14), Ru(2)–O(2)–Ru(3) 75.1(4), O(1)–C(1)–O(2) 118(2), O(1)–C(1)–O(3) 114(2), and O(2)–C(1)–O(3) 128(2). (b) DFT-optimized structure of **7** (orange Ru; red O; and grey C) and selected (3,–1) b.c.p. (green) with density values at b.c.p. (potential energy density values in parentheses). Data in a.u.

tron density (ρ) at b.c.p. is higher and the potential energy density (V) is more negative for the Ru–(κ¹-O) interaction with respect to the Ru–(μ-O) ones. AIM data are reported in Fig. 8.

The Hirshfeld partial charges on the Ru atoms are strictly comparable and the average value is 0.105 a.u. The average value for the separated neutral $\{Ru_3(CO)_9\}$ fragment is similar, 0.078 a.u., but surprisingly slightly less positive. Charge decomposition analysis (CDA) indicates that CO_3^{2-} behaves as a donor towards $\{Ru_3(CO)_9\}$ by about 0.51 a.u., without back-donation. The increase of the electron density is drained by carbonyl ligands, as confirmed by population analyses. The average CO Hirshfeld charge in **7** is −0.122 a.u., while it is −0.020 a.u. in the related $\{Ru_3(CO)_{12}\}$ fragment. Overall, the computed data do not suggest any change in the formal oxidation state of the Ru atoms upon coordination of CO_3^{2-}.

Synthesis and molecular structure of $[Ru_3(CO)_9(NPPh_3)]^-$ (9)

The reaction of **6** with an excess of NaOH in DMSO under a CO atmosphere affords $[Ru_2(CO)_8]^{2-}$ (**8**) rather than **4**. Both the compounds contain Ru in the formal oxidation state −1, but **8** has a higher CO/Ru ratio (4) compared to **4** (CO/Ru = 3) in accordance with eqn (1). Compound **8** has been identified by IR spectroscopy and, moreover, its structure has been supported by the SC-XRD pattern of the new $[NEt_4]_2[Ru_2(CO)_8]$ salt (Fig. S12 in the ESI†).

$$[HRu_4(CO)_{12}]^{3-} + 4CO \leftrightarrow 2[Ru_2(CO)_8]^{2-} + H^+ \quad (1)$$

Interestingly, performing the reaction of **6** with NaOH ion DMSO in the presence of $[PPN]^+$ ions ($[PPN]^+ = [N(PPh_3)_2]^+$) afforded the new $[Ru_3(CO)_9(NPPh_3)]^-$ (**9**) cluster.

Compound **9** has been previously identified by IR and $^{31}P\{^1H\}$ NMR spectroscopy during the deprotonation of $[HRu_3(CO)_9(NPPh_3)]$ (**10**) which, in turn, was obtained from the reaction of $Ru_3(CO)_{12}$ with $Ph_3P{=}NSiMe_3$.[43] The molecular structure of **9** was determined by SC-XRD as its $[NEt_4][Ru_3(CO)_9(NPPh_3)]$ salt (Fig. 9). It consists of a triangular Ru_3 cluster with a μ_3-$NPPh_3$ ligand, six terminal carbonyls (two per each Ru atom) and three μ-CO ligands on three edges of the Ru_3 triangle. In agreement with the solid state structure, its FT-IR spectrum in solution and in the solid state shows ν_{CO} bands due to both terminal and edge bridging carbonyls. It must be remarked that two isomers of **10** have been structurally characterized, one displaying the same stereochemistry of the CO ligands as found in **9**, whereas the second isomer possesses only terminal carbonyls. It is well known that increasing the anionic charge of a carbonyl cluster favours the bridging mode of the CO ligands.[44,45] For instance, **1** and **2** contain only terminal CO ligands, whereas **3** and **4** contain three μ-CO ligands.

Cluster **9** is electron precise since it possesses 48 cluster valence electrons (CVE) [3 × 8 (3Ru) + 9 × 2 (9CO) + 1 × 5 (μ_3-$NPPh_3$) + 1 (charge)] as expected for a triangular cluster. The μ_3-$NPPh_3$ contributes 5 CVE if considered as a neutral ligand and 6 CVE if considered as a mono-anion. A computational analysis of **9** is included in the ESI.†

The $^{31}P\{^1H\}$ NMR spectrum of **9** in CD_2Cl_2 at 298 K displays a sharp singlet at δ_P 57.03 ppm, considerably deshielded compared to the starting $[PPN]^+$ ions (δ_P 21 ppm).

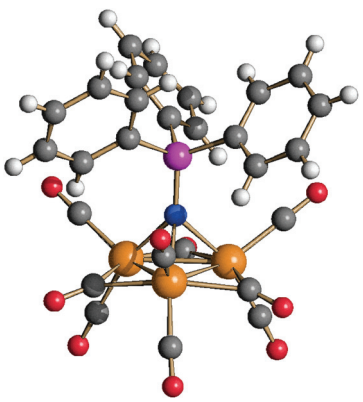

Fig. 9 Molecular structure of $[Ru_3(CO)_9(NPPh_3)]^-$ (**9**) (orange Ru; purple P; blue N; red O; grey C; and white H). Main bond distances (Å): Ru–Ru 2.7297(7), 2.7455(7) and 2.7471(7); Ru–N 2.125(5), 2.129(5) and 2.141(5); and N–P 1.597(5).

Conclusions

Synthesis, spectroscopic characterization and structural determination of $H_4Ru_4(CO)_{12}$ (**1**), $[H_3Ru_4(CO)_{12}]^-$ (**2**) and $[H_2Ru_4(CO)_{12}]^{2-}$ (**3**) hydride carbonyl clusters represented a milestone in cluster chemistry.[1,11,18,24,25] Spectroscopic evidence that they can be further deprotonated affording the $[HRu_4(CO)_{12}]^{3-}$ (**4**) mono-hydride tri-anion has been reported more than 40 years ago.[26,27] Nonetheless, **4** escaped up to now any effort devoted to its isolation and structural characterization. This is likely due to the experimental conditions employed during these attempts, rather than the intrinsic instability of **4**. Indeed, by carefully choosing the operational conditions and, in particular, by working in a highly polar aprotic solvent such as DMSO and using a strong base such as NaOH, it has been possible to convert **2** as well as $[HRu_3(CO)_{11}]^-$ (**6**) into **4**. This allowed its isolation and the determination of its structure by SC-XRD. Similar approaches have been recently adopted for the isolation of $[HFe_4(CO)_{12}]^{3-}$ starting from $[Fe_4(CO)_{13}]^{2-}$ or $[HFe_3(CO)_{11}]^-$,[9,10] as well as the synthesis of $[Fe_6C(CO)_{15}]^{4-}$ from $[Fe_6C(CO)_{16}]^{2-}$.[39] Thus, it seems that the use of strong bases in polar solvents such as DMSO or CH_3OH may be a general synthetic pathway towards highly reduced carbonylate clusters.

Two isomers of **4** rapidly exchange in solution, whereas a single isomer has been reported for $[HFe_4(CO)_{12}]^{3-}$.[9] The latter possesses the same C_{3v} structure with a μ_3-H found in the solid state structure of **4**. This might be due to the fact that, due to the larger size of Ru compared to Fe, there is more space in a $Ru_4(CO)_{12}$ tetrahedron rather than in $Fe_4(CO)_{12}$ in order to accommodate the hydride ligand on different sites. Indeed, it is well known that both $[Ru_4(CO)_{13}]^{2-}$ and $[Fe_4(CO)_{13}]^{2-}$ have a tetrahedral structure, which is retained in $[HRu_4(CO)_{13}]^-$, whereas $[HFe_4(CO)_{13}]^-$ shows a more open butterfly structure.[15–17] Nonetheless, it must be remarked that **3** and $[H_2Fe_4(CO)_{12}]^{2-}$ are isostructural.[10]

Comparison of $[H_{4-n}Ru_4(CO)_{12}]^{n-}$ (n = 0–3) and $[H_{4-n}Fe_4(CO)_{12}]^{n-}$ (n = 2–3) indicates that Ru prefers less charged poly-hydride species, whereas more charged anions are favored in the case of Fe. This may be explained by assuming higher basicity for the Ru cluster anions compared to the related Fe species. Indeed, **4** is easily protonated to **3**, whereas the protonation of $[HFe_4(CO)_{12}]^{3-}$ to $[H_2Fe_4(CO)_{12}]^{2-}$ requires strictly controlled conditions. Moreover, there is no evidence of less charged Fe poly-hydrides of the type $[H_3Fe_4(CO)_{12}]^-$ and $H_4Fe_4(CO)_{12}$.

These findings further corroborate the tendency of Ru toward the formation of poly-hydride clusters. Somehow this is correlated with the involvement of Ru–H complexes, molecular carbonyl clusters and nanoparticles in catalytic processes using hydrogen.[28–38]

Experimental

General procedures

All reactions and sample manipulations were carried out using standard Schlenk techniques under nitrogen and in dried solvents. All the reagents were commercial products (Aldrich) of the highest purity available and used as received. Analyses of C, H and N were performed using a Thermo Quest Flash EA 1112NC instrument. IR spectra were recorded using a PerkinElmer Spectrum One interferometer in CaF_2 cells. ^1H, $^{13}C\{^1H\}$ and $^{31}P\{^1H\}$ NMR measurements were performed using a Varian Mercury Plus 400 MHz instrument. The proton and carbon chemical shifts were referenced to the non-deuterated aliquot of the solvent. The phosphorus chemical shifts were referenced to external H_3PO_4 (85% in D_2O). Structure drawings were performed using SCHAKAL99.[46]

Synthesis of $[NEt_4][HRu_3(CO)_{11}]$ (6)[47]

$$RuCl_3 \cdot 3H_2O \xrightarrow[\substack{CH_3OH \\ p(CO):60\ atm \\ 120\,^\circ C,\ 14\ h}]{\overset{NaOMe}{[NEt_4]Br}} [NEt_4][HRu_3(CO)_{11}]$$

In a 100 mL autoclave, $RuCl_3{\cdot}3H_2O$ (1.57 g, 6 mmol), NaOMe (1.92 g, 35.6 mmol) and $[NEt_4]Br$ (0.630 g, 3 mmol) were dissolved in CH_3OH (40 mL). The autoclave was pressurized with CO (60 bar) and heated at 120 °C for 14 h. After cooling and venting, the deep red solution containing the already solid product was moved to a 250 mL Schlenk tube and filtered under a nitrogen atmosphere and the residue was washed with methanol (30 mL). Then, the solvent was removed from the filtrate under vacuum and the residue was extracted in CH_2Cl_2 (40 mL). The solvent was removed from the CH_2Cl_2 solution under reduced pressure. The residue was washed with water (2 × 30 mL) and toluene (2 × 20 mL) and then extracted with CH_2Cl_2 (30 mL). The product $[NEt_4][HRu_3(CO)_{11}]$ was obtained as a red solid with a yield of 75% after the removal of the solvent under reduced pressure. Crystals of $[NEt_4][HRu_3(CO)_{11}]$ suitable for SC-XRD can be obtained by slow diffusion of n-hexane on the CH_2Cl_2 solution (yield 1.48 g, 85%).

$C_{19}H_{21}NO_{11}Ru_3$ (742.583): calcd (%): C 30.73, H 2.85, N 1.89; found: C 30.91, H 2.62, N 2.05.

IR (CH_2Cl_2, 298 K) ν_{CO}: 2016(vs), 1987(s), 1952(m) cm^{-1}.

^1H NMR (acetone-d^6, 298 K) δ (hydride region): −12.51 ppm.

Synthesis of $[NEt_4]_3[HRu_4(CO)_{12}]$ (4) and $[NEt_4]_2[Ru_3(CO)_9(CO_3)]$ (7)

$$[NEt_4][HRu_3(CO)_{11}] \xrightarrow[\substack{DMSO \\ r.t.,\ 3\ days}]{NaOH} [HRu_4(CO)_{12}]^{3-} \xrightarrow[iPrOH]{} [NEt_4]_3[HRu_4(CO)_{12}]$$

NaOH (0.800 g, 200 mmol) was added as a solid to a solution of $[NEt_4][HRu_3(CO)_{11}]$ (0.550 g, 0.741 mmol) in DMSO (10 mL). The resulting mixture was stirred at room temperature for 3 days. The crude product was precipitated by the addition of iPrOH (100 mL) and the solid was recovered by filtration, washed with iPrOH (30 mL), and dried under reduced pressure. The orange solid was further washed with toluene (15 mL), THF (15 mL), and extracted in acetone (15 mL). The acetone solution was layered with n-hexane, affording crystals

of $[NEt_4]_2[Ru_3(CO)_9(CO_3)]$ suitable for SC-XRD (yield 0.175 g, 27%). Then, the residue was extracted in acetonitrile (15 mL) and layered with *n*-hexane and diisopropyl ether, affording crystals of $[NEt_4]_3[HRu_4(CO)_{12}]$ suitable for SC-XRD (yield 0.349 g, 58%).

$[NEt_4]_2[Ru_3(CO)_9(CO_3)]$ (4). IR (CH_3CN, 298 K) ν_{CO}: 1938(vs), 1907(s), 1757(m) cm^{-1}. IR (Nujol, 298 K) ν_{CO}: 1984(m), 1957(vs)(m), 1931(m), 1912(s), 1761(s) cm^{-1}. $^{13}C\{^1H\}$ NMR (Acetone-d^6, 298 K) δ (carbonyl region): 223.2 (CO), 217.7 (CO), 166.9 (CO_3) ppm.

$[NEt_4]_3[HRu_4(CO)_{12}]$ (7). IR (CH_3CN, 298 K) ν_{CO}: 1928(s), 1898(vs), 1855(m), 1714(m) cm^{-1}. IR (Nujol, 298 K) ν_{CO}: 1934(m), 1860(s)(m), 1744(w) cm^{-1}. ^1H NMR (CD_3CN, 298 K) δ (hydride region): −17.65 (br) ppm. ^1H NMR (CD_3CN, 273 K) δ (hydride region): −18.00 (coalescence) ppm. ^1H NMR (CD_3CN, 248 K) δ (hydride region): −18.43, −15.75 ppm. ^1H NMR (DMF-d^7, 298 K) δ (hydride region): −17.95 (br) ppm. ^1H NMR (DMF-d^7, 273 K) δ (hydride region): (coalescence). ^1H NMR (DMF-d^7, 248 K) δ (hydride region): −18.04, −15.32 ppm. ^1H NMR (DMF-d^7, 223 K) δ (hydride region): −17.90, −15.16 ppm. $^{13}C\{^1H\}$ NMR (CD_3CN, 298 K) δ (carbonyl region): 226 (br) ppm. $^{13}C\{^1H\}$ NMR (CD_3CN, 273 K) δ (carbonyl region): 225.0 (coalescence) ppm. $^{13}C\{^1H\}$ NMR (DMF-d^7, 298 K) δ (carbonyl region): 225.2 (br) ppm. $^{13}C\{^1H\}$ NMR (DMF-d^7, 273 K) δ (carbonyl region): 224.0 (coalescence) ppm. $^{13}C\{^1H\}$ NMR (DMF-d^7, 223 K) δ (carbonyl region): 268.7, 213.4, 213.0, 201.7 (C_{3v} isomer), 277.8, 276.7 (C_s isomer; the resonances of the terminal CO ligands could not be resolved) ppm.

Optimized synthesis of $[NEt_4]_3[HRu_4(CO)_{12}]$(4)

$[NEt_4][HRu_3(CO)_{11}]$ (0.700 g, 0.943 mmol) was stirred at room temperature with 1.50 g of freshly powdered KOH suspended in 10 mL of DMSO for 16 h. The orange solution decanted from KOH powder was added dropwise to a stirred solution of $[NEt_4]Br$ (2.00 g) in H_2O (15 mL) and iPrOH (150 mL). The crude compound precipitated immediately as an orange powder. The solid was obtained by filtration and vacuum dried. Then, the solid was washed with acetone (10 mL) and the product extracted in CH_3CN was identified as $[NEt_4]_3[HRu_4(CO)_{12}]$ by means of NMR and IR spectroscopy (yield 0.616 g, 77%).

$C_{36}H_{61}N_3O_{12}Ru_4$ (1132.15): calcd (%): C 38.19, H 5.43, N 3.71; found: C 38.31, H 5.07, N 3.49.

Synthesis of $[NEt_4][Ru_3(CO)_9(NPPh_3)]$ (9)

$$[PPN][HRu_3(CO)_{11}] \xrightarrow[DMSO]{NaOH} \xrightarrow{[NEt_4]Br} [NEt_4][Ru_3(CO)_9(NPPh_3)]$$

NaOH (0.950 g, 23.8 mmol) was added as a solid to a solution of $[PPN][HRu_3(CO)_{11}]$ (0.670 g, 0.582 mmol) in DMSO (10 mL) and the resulting mixture was stirred at room temperature overnight. The crude product was filtered and the solution was precipitated by the addition of a saturated solution of $[NEt_4]Br$

Table 4 Crystal data and experimental details for $[NEt_4][HRu_3(CO)_{11}]$, $[NEt_4]_2[Ru_2(CO)_8]$, $[NEt_4][Ru_3(CO)_9(NPPh_3)]$, $[NEt_4]_3[HRu_4(CO)_{12}]$ and $[NEt_4]_2[Ru_3(CO)_9(CO_3)]$

	$[NEt_4][HRu_3(CO)_{11}]$	$[NEt_4]_2[Ru_2(CO)_8]$	$[NEt_4][Ru_3(CO)_9(NPPh_3)]$	$[NEt_4]_3[HRu_4(CO)_{12}]$	$[NEt_4]_2[Ru_3(CO)_9(CO_3)]$
Formula	$C_{19}H_{21}NO_{11}Ru_3$	$C_{24}H_{40}N_2O_8Ru_2$	$C_{35}H_{35}N_2O_9PRu_3$	$C_{36}H_{61}N_3O_{12}Ru_4$	$C_{26}H_{40}N_2O_{12}Ru_3$
f_w	742.58	686.72	961.83	1132.15	875.81
T, K	100(2)	100(2)	100(2)	293(2)	100(2)
λ, Å	0.71073	0.71073	0.71073	0.71073	0.71073
Crystal system	Monoclinic	Monoclinic	Triclinic	Monoclinic	Monoclinic
Space group	$P2_1/c$	$P2_1/n$	$P\bar{1}$	$P2_1/n$	$P2_1/c$
a, Å	12.3458(10)	9.5198(6)	11.1727(11)	12.9763(8)	16.5638(16)
b, Å	11.7217(9)	13.7870(8)	11.9062(12)	19.4012(12)	10.2807(10)
c, Å	17.4163(15)	11.8620(7)	14.3383(14)	18.0370(11)	19.8070(19)
α, °	90	90	90.095(3)	90	90
β, °	97.810(3)	113.085(2)	99.075(3)	97.884(2)	105.465(3)
γ, °	90	90	100.292(3)	90	90
Cell volume, $Å^3$	2497.0(4)	1432.21(15)	1852.3(3)	4498.0(5)	3250.8(5)
Z	4	2	2	4	4
D_c, g cm^{-3}	1.975	1.592	1.725	1.672	1.790
μ, mm^{-1}	1.847	1.100	1.305	1.375	1.436
F(000)	1448	700	956	2280	1752
Crystal size, mm	0.22×0.18×0.14	0.24×0.21×0.19	0.18×0.12×0.11	0.14×0.12×0.11	0.16×0.14×0.10
θ limits, °	1.665–26.996	2.380–27.994	1.439–25.099	1.549–26.036	2.134–25.074
Index ranges	$-15 \le h \le 15$	$-12 \le h \le 12$	$-13 \le h \le 13$	$-15 \le h \le 15$	$-19 \le h \le 19$
	$-14 \le k \le 14$	$-18 \le k \le 18$	$-14 \le k \le 14$	$-23 \le k \le 23$	$-12 \le k \le 12$
	$-22 \le l \le 22$	$-15 \le l \le 15$	$-17 \le l \le 17$	$-22 \le l \le 22$	$-23 \le l \le 23$
Reflections collected	30401	31227	23609	56877	49201
Independent reflections	5447 [R_{int} = 0.0938]	3453 [R_{int} = 0.0377]	6537 [R_{int} = 0.0604]	8833 [R_{int} = 0.0815]	5706 [R_{int} = 0.1011]
Completeness to θ_{max}	100.0%	100.0%	99.2%	100.0%	99.1%
Data/restraints/parameters	5447/0/314	3453/0/167	6537/414/482	8833/825/647	5706/252/380
Goodness of fit on F^2	1.042	1.084	1.172	1.157	1.330
R_1 ($I > 2\sigma(I)$)	0.0403	0.0145	0.0521	0.0879	0.1398
wR_2 (all data)	0.0837	0.0355	0.0993	0.1983	0.3260
Largest diff. peak and hole, e $Å^{-3}$	1.156/−1.005	0.292/−0.355	1.438/−2.126	2.194/−1.663	2.880/−2.865

in H_2O. The solid obtained was recovered by filtration, washed with H_2O (40 mL), toluene (20 mL) and 2-propanol (20 mL), and then extracted with CH_2Cl_2 (15 mL). Crystals of $[NEt_4][Ru_3(CO)_9(NPPh_3)]$ suitable for SC-XRD were obtained by layering *n*-pentane on the CH_2Cl_2 solution (yield 0.352 g, 63%).

$C_{35}H_{35}N_2O_9PRu_3$ (961.83): calcd (%): C 43.71, H 3.67, N 2.91; found: C 43.56, H 3.38, N 3.11.

IR (CH_2Cl_2, 298 K) ν_{CO}: 2016(w), 1990(s), 1959(vs), 1926(m), 1750(m) cm^{-1}.

IR (Nujol, 298 K) ν_{CO}: 2018(w), 1979(ms), 1961(s), 1941(m), 1907(mw), 1890(mw), 1772(m), 1746(s) cm^{-1}.

$^{31}P\{^1H\}$ NMR (CD_2Cl_2, 298 K) δ: 57.03 ppm.

$^{13}C\{^1H\}$ NMR (CD_2Cl_2, 298 K) δ (carbonyl region): 221.5 ppm.

X-ray crystallographic study

Crystal data and collection details for $[NEt_4][HRu_3(CO)_{11}]$, $[NEt_4][Ru_3(CO)_9(NPPh_3)]$, $[NEt_4]_2[Ru_2(CO)_8]$, $[NEt_4]_3[HRu_4(CO)_{12}]$ and $[NEt_4]_2[Ru_3(CO)_9(CO_3)]$ are reported in Table 4. The diffraction experiments were carried out on a Bruker APEX II diffractometer equipped with a PHOTON2 detector using Mo–Kα radiation. Data were corrected for Lorentz polarization and absorption effects (empirical absorption correction SADABS).[48] Structures were solved by direct methods and refined by full-matrix least-squares based on all data using F^2.[49] Hydrogen atoms were fixed at calculated positions and refined using a riding model. All non-hydrogen atoms were refined with anisotropic displacement parameters, unless otherwise stated.

Computational details

Geometry optimizations of the clusters were performed in the gas phase using the range-separated hybrid DFT functional ωB97X.[50] The basis set used was Ahlrichs'def2 split-valence, with relativistic ECP for Ru.[51] The "restricted" approach was used in all the cases. The software used was Gaussian 09.[52] The output was used for AIM and Mayer analyses,[53] performed using the Multiwfn software, version 3.5.[54] The Cartesian coordinates of the DFT-optimized structures are obtained in a separate .xyz file.

Conflicts of interest

There are no conflicts to declare.

Acknowledgements

We thank the University of Bologna for financial support.

References

1 C. Cesari, J.-H. Shon, S. Zacchini and L. A. Berben, *Chem. Soc. Rev.*, 2021, **50**, 9503–9539.
2 S. Zacchini, *Eur. J. Inorg. Chem.*, 2011, 4125–4145.
3 W. Hieber and F. Leutert, *Die Naturwissenschaften*, 1931, **19**, 360–361.
4 J. J. Brunet, *Chem. Rev.*, 1990, **90**, 1041–1059.
5 J. Lewis and P. R. Raithby, *J. Organomet. Chem.*, 1995, **500**, 227–237.
6 (*a*) C. R. Eady, B. F. G. Johnson and J. Lewis, *J. Chem. Soc., Dalton Trans.*, 1977, 838–844; (*b*) S. A. R. Knox, J. W. Koepke, M. A. Andrews and J. Lewis, *J. Am. Chem. Soc.*, 1975, **97**, 3942–3947.
7 N. N. Greenwood and A. Earnshaw, *Chemistry of the Elements*, Butterworth-Heinemann, Oxford, 1984.
8 *The Chemistry of Metal Cluster Complexes*, ed. D. F. Shriver, H. D. Kaesz and R. D. Adams, VCH, New York, 1990.
9 C. Femoni, M. C. Iapalucci, G. Longoni, S. Zacchini and S. Zarra, *Inorg. Chem.*, 2009, **48**, 1599–1605.
10 C. Femoni, M. C. Iapalucci, G. Longoni and S. Zacchini, *Dalton Trans.*, 2011, **40**, 8685–8694.
11 C. Cesari, M. Bortoluzzi, C. Femoni, M. C. Iapalucci and S. Zacchini, *Dalton Trans.*, 2021, **50**, 9610–9622.
12 (*a*) L. F. Dahl and J. F. Blount, *Inorg. Chem.*, 1965, **4**, 1373–1375; (*b*) E. Isikola, T. A. Pakkanen, T. T. Pakkanen and T. Venalainen, *Acta Chem. Scand.*, 1983, **37**, 125–130.
13 (*a*) Y.-C. Liu, W.-Y. Yeh, G.-H. Lee and S.-M. Penn, *Organometallics*, 2003, **20**, 4163–4166; (*b*) F. Furno, T. Fox, M. Alfonso and H. Berke, *Eur. J. Inorg. Chem.*, 2001, 1559–1565; (*c*) J. A. Cabeza, M. Damonte, P. Garciá-Álvarez and E. Pérez-Carreño, *Chem. Commun.*, 2013, **49**, 2813–2815.
14 J. A. Krause, U. Siriwardane, T. A. Salupo, J. R. Wermer, D. W. Knoeppel and S. G. Shore, *J. Organomet. Chem.*, 1993, **454**, 263–271.
15 M. Manassero, M. Sansoni and G. Longoni, *J. Chem. Soc., Chem. Commun.*, 1976, 919–920.
16 (*a*) J. A. Jensen, D. E. Fjare and W. L. Gladfelter, *Inorg. Chem.*, 1983, **22**, 1250–1253; (*b*) S. V. Osintseva, N. A. Shtel'tser, A. S. Peregudov, A. Z. Kreindlin and F. M. Dolgushin, *Polyhedron*, 2018, **148**, 147–160.
17 P. A. Dawson, B. F. G. Johnson, J. Lewis, D. A. Kaner and P. R. Raithby, *J. Chem. Soc., Chem. Commun.*, 1980, 961–962.
18 (*a*) R. Suter, A. A. Bhattacharyya, L.-Y. Hsu, J. A. Krause Bauer and S. G. Shore, *Polyhedron*, 1998, **17**, 2889–2897; (*b*) C. E. Ellul, J. P. Lowe, M. F. Mahon, P. R. Raithby and M. K. Whittlesey, *Dalton Trans.*, 2018, **47**, 4518–4523.
19 B. F. G. Johnson, J. Lewis, P. R. Raithby, G. M. Sheldrick and G. Süss, *J. Organomet. Chem.*, 1978, **162**, 179–187.
20 P. J. Bailey, M. A. Beswick, B. F. G. Johnson, J. Lewis, M. McPartlin, P. R. Raithby and M. C. Ramirez de Arellano, *J. Chem. Soc., Dalton Trans.*, 1996, 3515–3520.
21 D. Braga, J. Lewis, B. F. G. Johnson, M. McPartlin, W. J. H. Nelson and M. D. Vargas, *J. Chem. Soc., Chem. Commun.*, 1983, 241–243.
22 T. Beringhelli, E. Cairati, C. Dragonetti, S. Galli, E. Lucentini, D. Roberto, A. Sironi and R. Ugo, *Inorg. Chim. Acta*, 2003, **354**, 79–89.
23 C. Femoni, M. C. Iapalucci, F. Kaswalder, G. Longoni and S. Zacchini, *Coord. Chem. Rev.*, 2006, **250**, 1580–1604.

24 (*a*) M. McPartlin and W. J. H. Nelson, *J. Chem. Soc., Dalton Trans.*, 1986, 1557–1563; (*b*) P. F. Jackson, B. F. G. Johnson, J. Lewis, M. McPartlin and W. J. H. Nelson, *J. Chem. Soc., Chem. Commun.*, 1978, 920–921; (*c*) C. E. Ellul, M. G. Mahon, O. Saker and M. K. Whittlesey, *Angew. Chem., Int. Ed.*, 2007, **46**, 6343–6345.
25 R. D. Wilson, S. M. Wu, R. A. Love and R. Bau, *Inorg. Chem.*, 1978, **17**, 1271–1280.
26 K. E. Inkrott and S. G. Shore, *Inorg. Chem.*, 1979, **18**, 2817–2821.
27 A. A. Bhattacharyya, C. C. Nagel and S. G. Shore, *Organometallics*, 1983, **2**, 1187–1193.
28 G. Hogarth, S. E. Kabir and E. Nordlander, *Dalton Trans.*, 2010, **39**, 6153–5174.
29 M. Zaun, A. Goeppert, R. May, R. Haiges, G. K. S. Prakash and G. A. Olah, *ChemSusChem*, 2011, **4**, 1241–1248.
30 A. F. Abdel-Magied, Y. Theibich, A. K. Singh, A. Rahaman, I. Doverbratt, A. K. Raha, M. Haukka, M. G. Richmond and E. Nordlander, *Dalton Trans.*, 2020, **49**, 4244–4256.
31 V. Moberg, R. Duquesne, S. Contaldi, O. Röhrs, J. Nachtigall, L. Damoense, A. T. Hutton, M. Green, M. Monari, D. Santelia, M. Haukka and E. Nordlander, *Chem. – Eur. J.*, 2012, **18**, 12458–12478.
32 M. Shieh, Y.-Y. Chu, L.-F. Jang and C.-H. Ho, *Inorg. Chem.*, 2014, **53**, 4284–4286.
33 U. Matteoli, M. Bianchi, P. Frediani, F. Piacenti, C. Botteghi and M. Marchetti, *J. Organomet. Chem.*, 1984, **263**, 243–246.
34 M. Bianchi, G. Menchi, P. Frediani, U. Matteoli and F. Piacenti, *J. Organomet. Chem.*, 1983, **247**, 89–94.
35 U. Matteoli, V. Beghetto and A. Scrivanti, *J. Mol. Catal. A: Chem.*, 1996, **109**, 45–50.
36 P. Homanen, R. Persson, M. Haukka, T. A. Pakkanen and E. Nordlander, *Organometallics*, 2000, **19**, 5568–5574.
37 (*a*) I. del Rosal, T. Gutmann, B. Walaszek, I. C. Gerber, B. Chaudret, H.-H. Limbach, G. Buntkowsky and R. Poteau, *Phys. Chem. Chem. Phys.*, 2011, **13**, 20199–20207; (*b*) T. Gutmann, I. del Rosal, B. Chaudret, R. Poteau, H.-H. Limbach and G. Buntkowsky, *ChemPhysChem*, 2013, **14**, 3026–3033.
38 T. Gutmann, B. Walaszek, X. Yeping, M. Wächtler, I. del Rosal, A. Grünberg, R. Poteau, R. Axet, G. Lavigne, B. Chaudret, H.-H. Limbach and G. Buntkowsky, *J. Am. Chem. Soc.*, 2010, **132**, 11759–11767.
39 M. Bortoluzzi, I. Ciabatti, C. Cesari, C. Femoni, M. C. Iapalucci and S. Zacchini, *Eur. J. Inorg. Chem.*, 2017, 3135–3143.
40 P. H. M. Budzelaar, *gNMR for Windows, NMR Simulation Program (5.0.6.0)*, IvorySoft, Adept Scientific, Letchworth, U.K, 2006.
41 J. W. Koepke, J. R. Johnson, S. A. R. Knox and H. D. Kaesz, *J. Am. Chem. Soc.*, 1975, **97**, 3947–3952.
42 L. Maurette, B. Donnadieu and G. Lavigne, *Angew. Chem., Int. Ed.*, 1999, **38**, 3707–3710.
43 R. Pattacini, G. Predieri, A. Tiripicchio, C. Mealli and A. D. Phillips, *Chem. Commun.*, 2006, 1527–1529.
44 F. Ragaini, J.-S. Song, D. L. Ramage, G. L. Geoffrey, G. A. P. Yap and A. L. Rheingold, *Organometallics*, 1995, **14**, 387–400.
45 C. Cesari, T. Funaioli, B. Berti, C. Femoni, M. C. Iapalucci, F. M. Vivaldi and S. Zacchini, *Inorg. Chem.*, 2021, **60**, 16713–16725.
46 E. Keller, *SCHAKAL99*, University of Freiburg, Germany, 1999.
47 A. Béguin, J. M. Soulié and G. Süss-Fink, *Inorg. Synth.*, 1998, **32**, 268–270.
48 G. M. Sheldrick, *SADABS, Program for empirical absorption correction*, University of Göttingen, Germany, 1996.
49 G. M. Sheldrick, *Acta Crystallogr., Sect. C: Struct. Chem.*, 2015, **71**, 3–8.
50 (*a*) Y. Minenkov, Å. Singstad, G. Occhipinti and V. R. Jensen, *Dalton Trans.*, 2012, **41**, 5526–5541; (*b*) J.-D. Chai and M. Head-Gordon, *Phys. Chem. Chem. Phys.*, 2008, **10**, 6615–6620; (*c*) I. C. Gerber and J. G. Ángyán, *Chem. Phys. Lett.*, 2005, **415**, 100–105.
51 (*a*) F. Weigend and R. Ahlrichs, *Phys. Chem. Chem. Phys.*, 2005, **7**, 3297–3305; (*b*) D. Andrae, U. Häußermann, M. Dolg, H. Stoll and H. Preuß, *Theor. Chim. Acta*, 1990, **77**, 123–141.
52 M. J. Frisch, G. W. Trucks, H. B. Schlegel, G. E. Scuseria, M. A. Robb, J. R. Cheeseman, G. Scalmani, V. Barone, B. Mennucci, G. A. Petersson, H. Nakatsuji, M. Caricato, X. Li, H. P. Hratchian, A. F. Izmaylov, J. Bloino, G. Zheng, J. L. Sonnenberg, M. Hada, M. Ehara, K. Toyota, R. Fukuda, J. Hasegawa, M. Ishida, T. Nakajima, Y. Honda, O. Kitao, H. Nakai, T. Vreven, J. A. Montgomery Jr., J. E. Peralta, F. Ogliaro, M. Bearpark, J. J. Heyd, E. Brothers, K. N. Kudin, V. N. Staroverov, R. Kobayashi, J. Normand, K. Raghavachari, A. Rendell, J. C. Burant, S. S. Iyengar, J. Tomasi, M. Cossi, N. Rega, J. M. Millam, M. Klene, J. E. Knox, J. B. Cross, V. Bakken, C. Adamo, J. Jaramillo, R. Gomperts, R. E. Stratmann, O. Yazyev, A. J. Austin, R. Cammi, C. Pomelli, J. W. Ochterski, R. L. Martin, K. Morokuma, V. G. Zakrzewski, G. A. Voth, P. Salvador, J. J. Dannenberg, S. Dapprich, A. D. Daniels, Ö. Farkas, J. B. Foresman, J. V. Ortiz, J. Cioslowski and D. J. Fox, *Gaussian 09, Revision C.01*, Gaussian Inc., Wallingford, CT, 2010.
53 (*a*) F. Jensen, *Introduction to Computational Chemistry*, Wiley, Chichester, 2nd edn, 2007; (*b*) C. J. Cramer, *Essentials of Computational Chemistry*, Wiley, Chichester, 2nd edn, 2004.
54 T. Lu and F. Chen, *J. Comput. Chem.*, 2012, **33**, 580–592.